

See discussions, stats, and author profiles for this publication at: <https://www.researchgate.net/publication/45718751>

Novel Melt-Processable Poly(ether ether ketone)(PEEK)/Inorganic Fullerene-like WS₂ Nanoparticles for Critical Applications

ARTICLE *in* THE JOURNAL OF PHYSICAL CHEMISTRY B · SEPTEMBER 2010

Impact Factor: 3.3 · DOI: 10.1021/jp105340g · Source: PubMed

CITATIONS

36

READS

41

5 AUTHORS, INCLUDING:



Mohammed Naffakh

Universidad Politécnica de Madrid

73 PUBLICATIONS 1,179 CITATIONS

[SEE PROFILE](#)



Ana M Diez-Pascual

Spanish National Research Council

61 PUBLICATIONS 960 CITATIONS

[SEE PROFILE](#)



I. Jiménez

Spanish National Research Council

114 PUBLICATIONS 2,001 CITATIONS

[SEE PROFILE](#)

Novel Melt-Processable Poly(ether ether ketone)(PEEK)/Inorganic Fullerene-like WS₂ Nanoparticles for Critical Applications

Mohammed Naffakh,^{*,†} Ana M. Díez-Pascual,[†] Carlos Marco,[†] Marián A. Gómez,[†] and Ignacio Jiménez[‡]

Departamento de Física e Ingeniería de Polímeros, Instituto de Ciencia y Tecnología de Polímeros, CSIC, c/Juan de la Cierva, 3, 28006, Madrid, Spain, and Instituto de Ciencia de Materiales de Madrid, CSIC, Campus de Cantoblanco, 28049 Madrid, Spain

Received: June 10, 2010; Revised Manuscript Received: July 22, 2010

The combination of high-performance thermoplastic poly(ether ether ketone) (PEEK) with inorganic fullerene-like tungsten disulfide (IF-WS₂) nanoparticles offers an attractive way to combine the merits of organic and inorganic materials into novel polymer nanocomposite materials. Here, we report the processing of novel PEEK/IF-WS₂ nanocomposites, which overcome the nanoparticle agglomerate formation and provide PEEK–particle interactions. The IF-WS₂ nanoparticles do not require exfoliation or modification, making it possible to obtain stronger, lighter materials without the complexity and processing cost associated with these treatments. The nanocomposites were fabricated by melt blending, after a predispersion step based on ball milling and mechanical treatments in organic solvent, which leads to the dispersion of individually IF-WS₂ nanoparticles in the PEEK matrix as confirmed by scanning electron microscopy. In order to determine the performance of the PEEK/IF-WS₂ nanocomposites for potential critical applications, particularly for the aircraft industry, we have extensively investigated these materials with a wide range of structural, thermal, and mechanical techniques using time-resolved synchrotron X-ray diffraction, thermogravimetric analysis, differential scanning calorimetry, dynamic-mechanical analysis, and tensile and impact tests as well as thermal measurements. Modulus, tensile strength, thermal stability, and thermal conductivity of PEEK exhibited remarkable improvement with the addition of IF-WS₂.

1. Introduction

In the past years, there has been a great deal of activity in the synthesis and development of high-performance and high-temperature polymers motivated by the need for advanced materials required for a diverse range of applications in the aerospace, automotive, and microelectronic industries. These applications often demand a unique combination of properties including high glass transition temperatures, toughness, good adhesion, oxidative and thermal stability, and low dielectric constant. In this regard, polymer–inorganic nanoparticles offer an attractive means to combine the merits of organic and inorganic materials of various architectures (e.g., spherical, tube, cube, platelike, fiber, wire, rods) into novel polymeric systems.^{1–7} Hybridization of such organic and inorganic is an important and evolutionary route for the growth of strong polymer–nanofiller interface in order to improve the thermal, mechanical, tribological, and optical properties of polymeric systems. Practically, it offers economic advantage and is versatile in nature. This can be explained by the low volume (1–10%) of nanofillers required to achieve properties which are comparable or even better than those achieved by conventional loadings (15–40%) of traditional fillers. The lowest loadings facilitate processing and reduce component weight. Also, this means higher strength to weight ratio which is very useful in case of automobile and aerospace industries to increase fuel economy.

However, many applications of high-performance and high-temperature polymers (e.g., poly(ether ether ketone)s, semicrystalline polyimides, etc.) are limited by the solubility and distribution of the nanoparticles in the polymer matrices. While these semicrystalline polymers offer tremendous opportunities due to the diverse range of useful properties (ductility, toughness, easy processing, thermal stability, and recyclability), this limitation has certainly impeded their advancement with respect to large-scale applications. Melt processing is obviously beneficial compared to solvent routes because it (1) is environmentally friendly (does not require handling dangerous solvents often associated with high performance polymers); (2) involves significantly shorter cycle times; (3) is easier to process; (4) is often economically more attractive; and (5) makes some large scale applications feasible. Another attractive feature desirable in these linear aromatic thermoplastic is the presence of a crystalline phase, which leads to substantial improvement in many properties, including solvent resistance, radiation stability, and partial retention and enhancement of certain mechanical properties much above the glass transition temperature. In this regard, new strategies such as the dispersion of inorganic fullerene-like materials (IF) are required to break through the performance ceiling of current nanocomposites. The revolutionary properties of inorganic fullerene-like nanoparticles (e.g., tungsten disulfide, IF-WS₂),⁸ such as high modulus and low friction coefficient, attributed to their small size, closed structure, and chemical inertness, make them potential candidates to improve the thermal, mechanical, and tribological properties of thermoplastic polymers, as has been shown for poly(ether ether ketone) coatings produced using aerosol-assisted deposition process⁹ as well as isotactic polypropylene (iPP)^{10,11} and

* To whom correspondence should be addressed. E-mail: mnaffakh@ictp.csic.es.

[†] Instituto de Ciencia y Tecnología de Polímeros, CSIC.

[‡] Instituto de Ciencia de Materiales de Madrid, CSIC.

polyphenylene sulfide (PPS)^{12–14} produced via melt blending, without using modifiers or surfactants. Fullerene-like nanoparticles have been shown to exhibit excellent solid lubrication behavior, suggesting many applications in, for example, the automotive and aerospace industries, home appliances, and recently for medical technology.¹⁵ Numerous development programs are in progress, some of them at a very advanced stage or even having made products. The first medical application (e.g., alleviating friction in orthodontic wires) was recently demonstrated,¹⁶ with numerous others to follow. Toxicological tests on the fullerene-like WS₂ nanoparticles concluded that they are safe.¹⁷ These findings open up vast opportunities for various potential applications in the field of polymer nanocomposites.

Since its introduction by the Imperial Chemical Industries (ICI) in the 1980s, PEEK has generated lot of industrial interest as one of the leading thermoplastic matrix candidate for use in automotive, oil and gas, healthcare, aircraft, semiconductor, fuel cell devices, and various industrial friction and wear components. The chemical structure of PEEK, consisting of an aromatic backbone molecular chain, interconnected by ketone and ether functional groups, confers stability at high temperatures (exceeding 300 °C), resistance to chemical and radiation damage, compatibility with many reinforcing agents (such as glass and carbon fibers), and greater strength (on a per mass basis) than many metals, making it highly attractive in critical industrial applications, such as aircraft, automotive, fuel cell energy, and medical implants.^{18–22}

The prime objective of this research is to develop and characterize novel PEEK/IF-WS₂ nanocomposites processed advantageously by the traditional melt processing technique. It is well-known that the properties of a crystalline polymer, including the thermodynamic, physical, or mechanical ones, depend on the details of the structure and morphology that evolve from the melt. Thus, detailed nanolevel investigation of processing/characterization along with the performance evaluation would give an insight into the structure–property–performance relationship of such nanocomposites.

2. Experimental Section

2.1. Materials and Processing.

Poly(ether ether ketone) (PEEK 150P) used in this study was provided in coarse powder form by Victrex plc, UK. This low-viscosity grade, the most suitable one for potential aircraft structural applications, presents the following physical characteristics: molecular weight (M_w) ~ 40 000 g/mol, glass transition (T_g) = 147 °C, melting temperature (T_m) = 345 °C, and density at 25 °C ($d_{25^\circ\text{C}}$) = 1.32 g/cm³. The IF-WS₂ nanoparticles (NanoLub) were provided by Nanomaterials (in Israel, ApNano Materials in USA). The particles are multifaced polyhedra with an apparent shape ranging from spheres to ellipsoids. The particle aspect ratio ranges between 1 (spheres) and 2.3, with a mean value of 1.4, standard deviation of 0.3 and a median of 1.36. The particle dimensions are in the range of 40–200 nm with a mean value of 80 nm, standard deviation of 30 nm and median of 75 nm.¹⁰ In our investigation, the ball milling strategy was only used to reduce the particle size of pure PEEK from millimeter to micrometer scale (i.e., ~5 μm), without the addition of IF-WS₂ nanoparticles. This process was performed at room temperature in a Restch MM 2000 vibratory ball mill, operating at maximum amplitude for 3 min. The cylinder had an internal volume of 8 cm³, and we employed two steel balls of Ø = 12 mm. Before the milling the thermoplastic polymer was dried at 120 °C for 4 h to minimize the effects of moistures.

Each mixture of PEEK and IF-WS₂ nanoparticles (0.1, 0.5, 1, and 2 wt %) was dispersed in a small volume of ethanol and

then homogenized by mechanical stirring and bath ultrasonication for approximately 10 min. Subsequently, the dispersion was partially dried in vacuum at 50 °C under a pressure of about 70 mbar for 24 h. The melt mixing of the resulting dispersions was performed using a Haake Rheocord 90 system operating at 380 °C and a rotor speed of 150 rpm for 20 min. In order to test the role of the previous preparation step, several concentrations of IF-WS₂ were introduced directly with PEEK by melt mixing without using ethanol. Then, the samples were pressed as films of 0.5 mm thickness in a hot-press system using two heating/cooling plates.

2.2. Characterization Techniques.

Scanning electron microscopy (SEM), thermogravimetric analysis (TGA), differential scanning calorimetry (DSC), and simultaneous small- and wide-angle X-ray scattering (SAXS/WAXS) were undertaken to analyze the morphological, thermal, and structural characteristics of the PEEK/IF-WS₂ nanocomposites. The dispersion of IF-WS₂ in the PEEK matrix was characterized using a Philips XL30 ESEM scanning electron microscope (SEM) equipped with an energy-dispersive X-ray (EDX) EDAX superUTW microanalytical system. The cryo-fractured film specimens were coated with a ~5 nm Au/Pd overlayer to avoid charging during electron irradiation. The thermal stability of the nanocomposites was analyzed by thermogravimetric analysis (TGA) using a Mettler TA-4000/TG-50 thermobalance with a heating rate of 20 °C/min from room temperature to 750 °C both in oxidizing (air) and inert (nitrogen) atmosphere. The crystallization and melting behavior of nanocomposites were investigated by differential scanning calorimetry using a Mettler TA4000/DSC30. The experiments were carried out in nitrogen atmosphere using approximately 12 mg of sample sealed in aluminum pans. Prior to the cooling and heating scans, the samples were held at 380 °C for 5 min to erase the thermal history of PEEK. Then, the crystallization of the samples under nonisothermal conditions was carried out by cooling from 380 to 30 °C. Four different crystallization experiments at cooling rates of at 2, 5, 10, and 15 °C/min were performed. Simultaneous SAXS/WAXS experiments using synchrotron radiation were performed at the A2 beamline of the HASYLAB synchrotron facility (DESY, Hamburg). The experiments were performed with monochromatic X-rays of 0.15 nm wavelength using a germanium single crystal as the dispersing element. The scattering was detected with a linear Gabriel detector. The sample to detector distance of SAXS was 2360 mm, and for WAXS was 135 mm. The scattering angle of the SAXS pattern was calibrated with the RTT (rat tail tendon), and that of the WAXS profile was calibrated with a PET standard. The maximum of the Lorentz-corrected SAXS diffractograms was used to calculate the long period ($L = 1/s_{\max}$) as a function of the temperature. L represents the sum of the average thickness of the crystal lamellae and of the interlamellar amorphous regions. Measurements were performed with acquisition time of 30 s (wait time 20 s and read time 10 s).

In addition, a wide range of mechanical testing methods were used to analyze the mechanical performance of the nanocomposites. The dynamic-mechanical behavior was studied using a dynamic mechanical analyzer (Mettler DMA861). The samples were cut in rectangular shapes with size of approximately 19.5 × 4 × 0.5 mm³ and mounted in a large tension clamp. The measurements were performed in the tensile mode at various frequencies (0.1, 1, and 10 Hz), in a temperature range between –130 and 260 °C with a heating rate of 2 °C/min. A dynamic force of 6 N oscillating at fixed frequency and amplitude of 30 μm was used. Tensile mechanical properties of the nanocom-

posites were measured with an INSTRON 4204 tester at room temperature 23 ± 2 °C and $50 \pm 5\%$ relative humidity, using a crosshead speed of 1 mm/min and a 1 kN compression load cell. Dog-bone specimens (Type V) were employed, as specified in the UNE-EN ISO 527-1 standard. All the samples were conditioned for 24 h before the measurements. At least five specimens for each type of naocomposite were tested to ensure reproducibility. Charpy notched impact strength measurements were carried out using a CEAST Fractovis dart impact tester. A hammer mass of 1.096 kg impacted at a constant velocity of 3.60 m s^{-1} and an energy of 7.10 J on notched specimen bars with dimensions of length 33 mm, width 10 mm, and thickness 3 mm, with a V-shape notch of tip radius 0.25 mm and depth 2 mm, as described in the UNE-EN ISO 179 standard. Measurements were performed at room temperature 23 ± 2 °C and $50 \pm 5\%$ relative humidity. The presented data correspond to the average value of at least seven test specimens.

Finally, thermal conductivity experiments were carried out with a THASYS Hukseflux thermal sensor equipped with a thin heater (THA01) and a measurement and control unit (MCU). To eliminate the problem of contact resistance, thin film samples (~ 0.5 mm thick) were immersed in glycerol. Thermal conductivity values were calculated from the heat flux and the differential temperature across the samples. At least three specimens for each composition were tested to report an average value.

3. Results and Discussion

3.1. Dispersion of IF-WS₂ in the PEEK Matrix. Nanocomposites can, in principle, incorporate nanoparticles (e.g., clays, organoclays, carbon nanotubes, etc.) in a number of ways including various in situ polymerization, solution, and latex methods. However, melt processing has involved the greatest interest because this is generally considered more economical and more flexible for formulation, and involves compounding and fabrication facilities commonly used in commercial practice.^{1,6} For most purposes, the dispersion of individual nanofillers in the polymer matrix is the desired goal of the formation process. However, this ideal morphology is frequently not achieved. Figure 1 shows SEM images of melt-processable PEEK/IF-WS₂ nanocomposites obtained from both direct and predisposition step in ethanol. It is clearly seen that the predisposition step is an efficient method for dispersing IF-WS₂ nanoparticles into the PEEK matrix. The apparent average size of the individual nanoparticles is about 110 nm, corresponding to a dispersion of individual IF particles or small clusters of 2–3 particles, which indicates that these nanoparticles are potential candidates for the preparation of new formulations based on high-performance thermoplastics like PEEK. Since particle size is an important factor in nucleation efficiency, proper particle dispersion is of paramount importance in property improvement.

3.2. Thermal Stability. Thermogravimetric analysis was performed in order to test the influence of these promising nanoparticles on the thermal stability of PEEK. The thermogravimetric curves for PEEK and PEEK/IF-WS₂ nanocomposites are shown in Figure 2 and the degradation tabulated data are summarized in Table 1. It can be observed that the thermal stability of PEEK increases with the addition of IF-WS₂, and the decomposition process of the PEEK components seems to be more complex in the presence of oxygen (i.e., overlapping of two degradation steps).^{23,24} The incorporation of the IF-WS₂ nanoparticles induces a remarkable thermal stabilization of the polymer matrix, with an increase of the initial degradation temperature (T_i) up to 60 °C (55 °C in the case of air

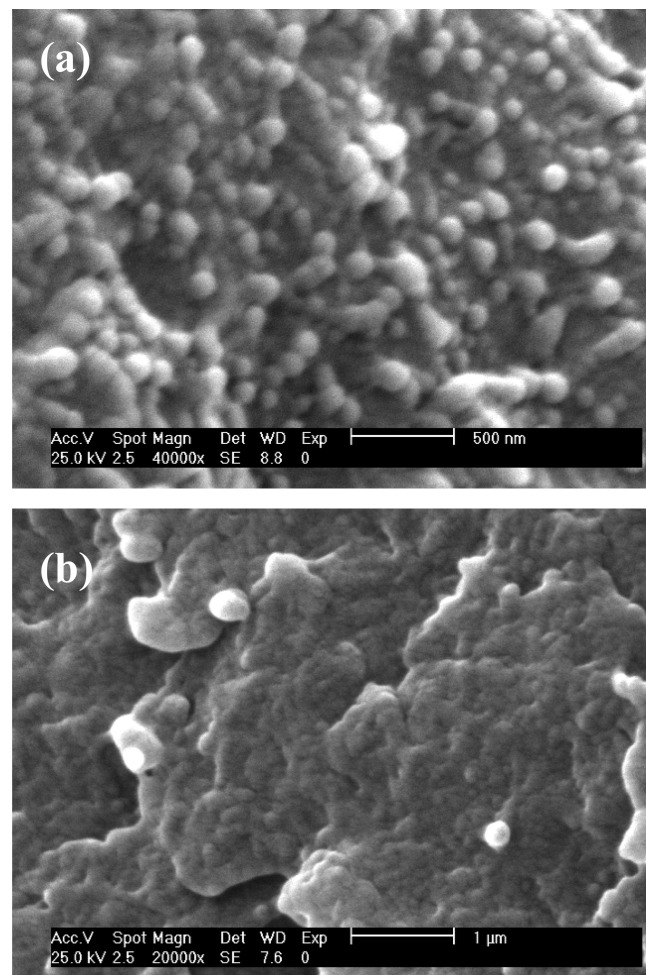


Figure 1. Melt-processable PEEK/IF-WS₂ (1 wt %) nanocomposites obtained from both (a) direct and (b) predisposition step in ethanol.

atmosphere). In the same way, the nanocomposites show a significant increase in thermal stability in terms of the maximum degradation rate temperatures (T_{mr}) compared to pure PEEK (e.g., T_{mr} of PEEK increase by 60 °C in nitrogen atmosphere). Moreover, the thermal stability of PEEK/IF-WS₂ nanocomposites is also influenced by the processing route. As shown in Table 1, the TGA temperature values of nanocomposites incorporating individual nanoparticles are higher than those obtained from direct mixing, suggesting the effective role of the predisposition step. These results show an important enhancement in the stability, in different environments, making the PEEK/IF-WS₂ nanocomposites highly attractive in critical industrial applications such as aeronautics.

3.3. Crystallization Behavior. The properties of a crystalline polymer including the thermodynamic, spectroscopic, physical, or mechanical ones depend on the details of the structure and morphology that evolve from the melt. Thus, understanding crystallization mechanisms is a key to understanding properties. For this reason, the crystallization of the PEEK/IF-WS₂ nanocomposites under dynamic conditions was carried out by cooling from 380 to 30 °C at different cooling rates. As the cooling rate increases, the crystallization exotherm broadens and shifts to lower temperatures for PEEK and PEEK/IF-WS₂ nanocomposites. This is directly related to the formation of smaller crystals with a wider distribution of crystallite sizes. However, the most relevant observation was the influence of IF-WS₂ concentration on the crystallization temperature of PEEK for a particular cooling rate (Figure 3). The addition of low concen-

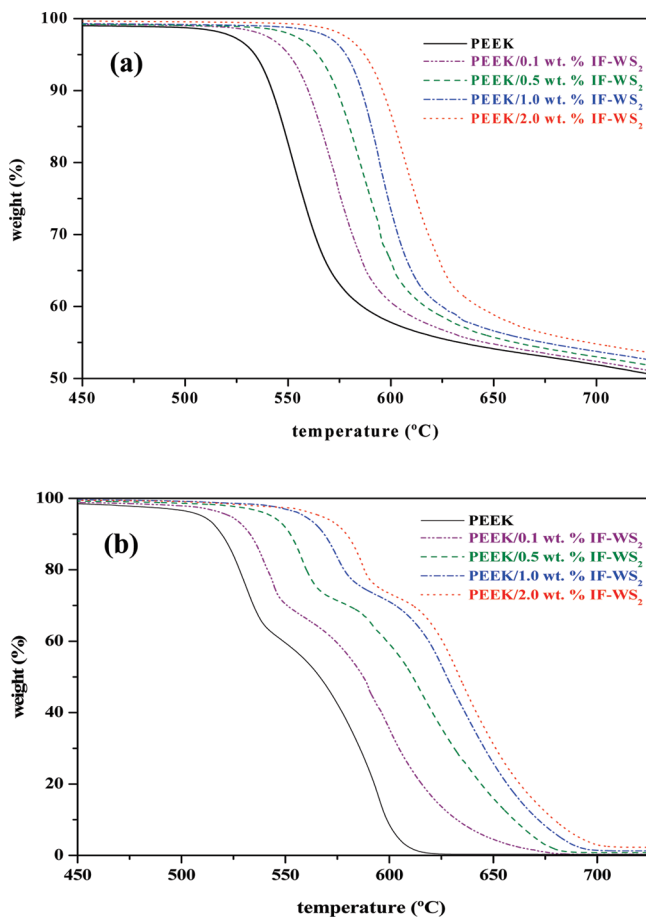


Figure 2. TGA curves of PEEK/IF-WS₂ nanocomposites (a) in nitrogen and (b) oxygen atmospheres.

TABLE 1: TGA Data under Nitrogen and Oxygen Atmosphere of PEEK/IF-WS₂ Nanocomposites Obtained during Heating at 20 °C/min^a

IF-WS ₂ content (%)	air			nitrogen		
	T _i (°C)	T ₁₀ (°C)	T _{mrl,II} (°C)	T _i (°C)	T ₁₀ (°C)	T _{mrl} (°C)
0	478	520	528/586	516	541	554
0.1	499	532	540/603	535	559	573
0.5	519	551	559/618	548	572	588
1	537	567	575/628	565	586	599
2	533	579	585/633	575	594	613
0.1 ^b	486	527	532/597	527	548	562
1 ^b	521	558	563/620	552	580	591

^a The displayed temperatures are T_i, initial degradation temperature obtained at 2% weight loss; T₁₀, temperature for 10% weight loss; and T_{mrl}, temperature corresponding to the maximum rate of weight loss. ^b Nanocomposites obtained from direct mixing.

trations of IF-WS₂ (i.e., less than or equal to 0.5 wt %) leads to a slight increase in crystallization temperature of PEEK, which may imply that the nucleation of PEEK crystals is favored by the IF-WS₂ nanoparticles. This observation is reproducible for nanocomposites crystallized at different cooling rates as can be seen in Figure 4 and is quite common compared with the effect of other nanofillers on polymer crystallization.^{6,25,26} It is generally accepted that the addition of nanoparticles into the polymer matrix favors heterogeneous nucleation and thus is expected to make the molecular chains of polymer matrix easier to crystallize and increase the crystallization rate of the nanocomposites in contrast to that of neat polymer (i.e., increase of peak crystallization temperature of polymer matrix). However, the further

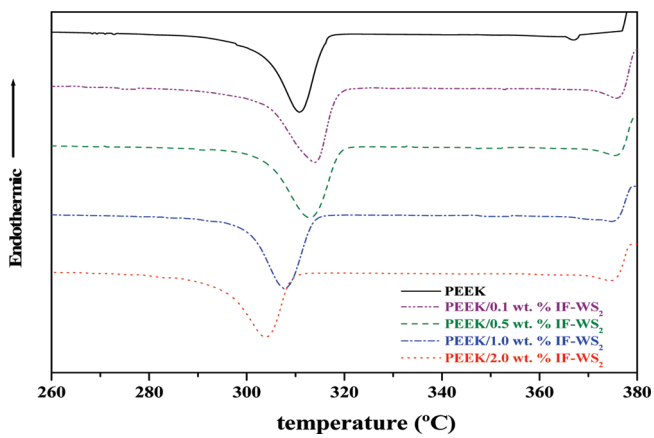


Figure 3. DSC thermograms of dynamic crystallization of PEEK/IF-WS₂ nanocomposites from melt to room temperature at 10 °C/min.

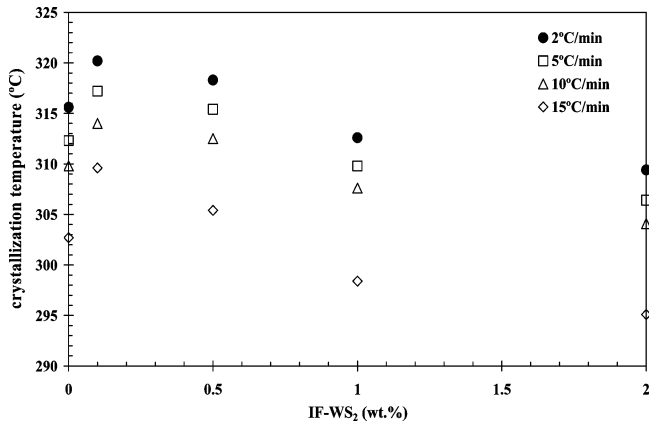


Figure 4. Crystallization temperatures of PEEK/IF-WS₂ nanocomposites obtained at various cooling rates.

addition of IF-WS₂ causes a drastic change from promotion to retardation of the crystallization of PEEK, without variation of the crystallinity (i.e., around 43%). This behavior is reproducible for the nanocomposites obtained from direct mixing, which indicates that the variation of the crystallization rate of PEEK is related to the increase of the concentration of IF-WS₂ in PEEK/IF-WS₂ (e.g., T_{c,PEEK} = 311 °C, T_{c,0.1wt%} = 313 °C, and T_{c,1wt%} = 305 °C at cooling rate of 10 °C min⁻¹). The decrease in the crystallization temperature of PEEK with increasing IF-WS₂ content suggests that IF-WS₂ does not act as nucleating agent in PEEK/IF-WS₂ nanocomposites. In this case, the presence of these nanoparticles may impede the diffusion and arrangement of the long polymer chains and thereby postpone the overall crystallization process. Similar behavior has been reported recently for other formulation like PEEK/nano-SiO₂ and compatibilized PEEK/SWNT with polysulfones using a ball milling technique.^{27,28} However, no variation of the crystallization rate of PEEK was observed with increasing SWNT content for the PEEK/SWNT nanocomposites incorporating pure SWNT as well as SWNT modified with PEI as a compatibilizer.^{29,30}

In order to understand the experimental data obtained for the crystallization behavior of PEEK/IF-WS₂ nanocomposites, we analyzed the DSC curves at different cooling rates in order to determine the kinetic parameters (i.e., nucleation activity, activation energy, etc.). The physicochemical changes during an exothermic event in DSC are complex and involve multistep processes occurring simultaneously at different rates. It is well-known that the crystallization from the melt state involves simultaneous nucleation and growth during the initial stage,

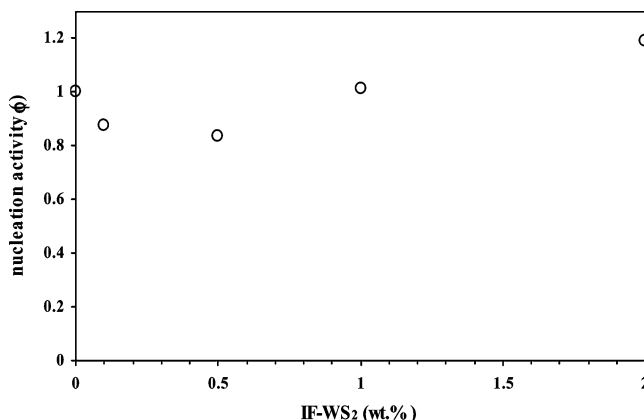


Figure 5. Variation of the nucleation activity of IF-WS₂ with concentration for PEEK/IF-WS₂ nanocomposites.

while from the region nearer to the crystallization peak the process is mainly dominated by growth; i.e., nucleation if at all exists becomes negligible from the region nearer to the crystallization peak and the process becomes isokinetic. Dobreva and Gutzow^{31,32} suggested a simple method for calculating the nucleation activity (φ) decreases with the addition of fillers. It is known that the nucleation activity (φ) decreases with the addition of fillers. If the foreign substrate is extremely active, φ approaches 0, while for inert particles φ approaches 1. For homogeneous nucleation, the heating rates can be written as

$$\ln \varphi = A - \frac{B}{\Delta T_p^2} \quad (1)$$

while for the heterogeneous case

$$\ln \varphi = A - \frac{B^*}{\Delta T_p^2} \quad (2)$$

$$\varphi = \frac{B^*}{B} \quad (3)$$

where ϕ is the heating rate, A is a constant, and ΔT_p is the difference between the melting temperature and the temperature corresponding to the peak temperature of the DSC cold-crystallization curves. B is a parameter that can be calculated from the following equation:

$$B = \frac{\omega \sigma^3 V_m^2}{3n k_B T_m^0 \Delta S_m^2} \quad (4)$$

where ω is a geometrical factor, σ is the specific energy, V_m is the molar volume of the crystallizing substance, n is the Avrami exponent, ΔS_m is the entropy of melting, k_B is the Boltzmann constant, and T_m^0 is the infinite crystal melting temperature. Therefore, the nucleation activity φ was simply calculated by the ratio of the slopes of $\log \phi$ vs $1 = \Delta T^2$ with and without IF-WS₂ filler by using eqs 1 and 2. From the slopes of these lines, the values of B and B^* can be calculated as shown in Figure 5. The addition of low concentrations of IF-WS₂ (i.e., less than or equal to 0.5 wt %) reduces the values of φ , which indicates that IF-WS₂ was acting effectively as a nucleating agent in the PEEK matrix. However, the further addition of IF-

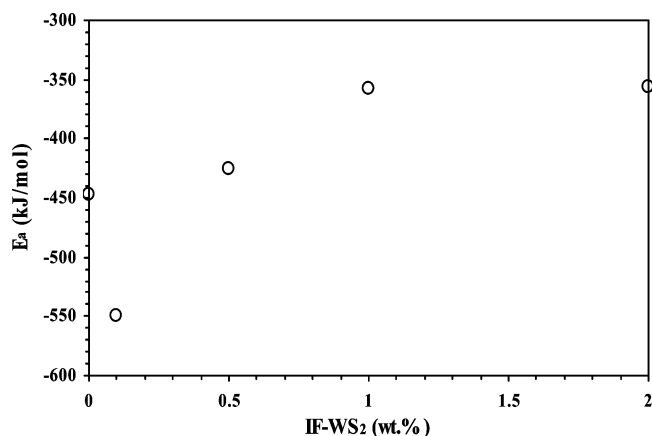


Figure 6. Variation of the effective energy barrier of PEEK crystallization with IF-WS₂ concentration for PEEK/IF-WS₂ nanocomposites.

WS₂ leads to a negative effect on the nucleation process because their values are close to 1 (i.e., 1 and 1.2 for nanocomposites with 1 and 2 wt % of IF-WS₂), implying that IF-WS₂ is not nucleating the PEEK matrix. This dependence of the nucleating activity of IF-WS₂ on the PEEK matrix justifies the variation of the crystallization temperature of PEEK with the content of IF-WS₂ (Figures 3 and 4).

On the other hand, the crystallization activation energy, or effective energy barrier ΔE , can be used to estimate the growth ability of the chain segments. The higher ΔE , the more difficult is the transport of macromolecular segments to the growing surface. Considering the variation of the peak temperature T_p with the heating rate ϕ , ΔE could be derived from the Kissinger equation through eq 5:³³

$$\ln\left(\frac{\phi}{T_p^2}\right) = \text{constant} - \frac{\Delta E}{RT_p} \quad (5)$$

where R is the universal gas constant, the rest of the parameters being described previously. From the plots of $\ln(\phi/T_p^2)$ vs $1 = T_p$, the values of ΔE for PEEK/IF-WS₂ nanocomposites can be calculated (Figure 6). In the same way, the values of ΔE evidenced by Kissinger analysis are also a unique manifestation of the composition-dependent crystallization behavior of PEEK. A drastic change from crystallization promotion (low ΔE) to crystallization retardation (higher ΔE) is observed as a function of the IF-WS₂ content. In this case, the increase in the ΔE indicates that the transport of the macromolecular segments to the growing surface of PEEK in the nanocomposite is difficult and crystallization is slower because of the inactive nucleating role of IF-WS₂ nanofillers.

To verify if the variation in the crystallization characteristics is accompanied by the modification of the crystalline structure of PEEK, we have monitored the crystallization process by *in situ* real-time SAXS/WAXS experiments using synchrotron radiation. Figure 7 shows the WAXS diffractograms recorded during the cooling process at a rate of 10 °C/min for PEEK/IF-WS₂ (2 wt %). The main Bragg reflections of the orthorhombic structure of PEEK are observed at 2θ angles of 18.7°, 20.6°, 22.9°, and 28.8°, associated to the diffraction of the (110), (111), (200), and (211) crystalline planes, respectively.^{34,35} The peaks in WAXS patterns of PEEK appear as soon as the material attains an appreciable degree of crystallinity. The appearance of these peaks relates well to the crystallization temperature

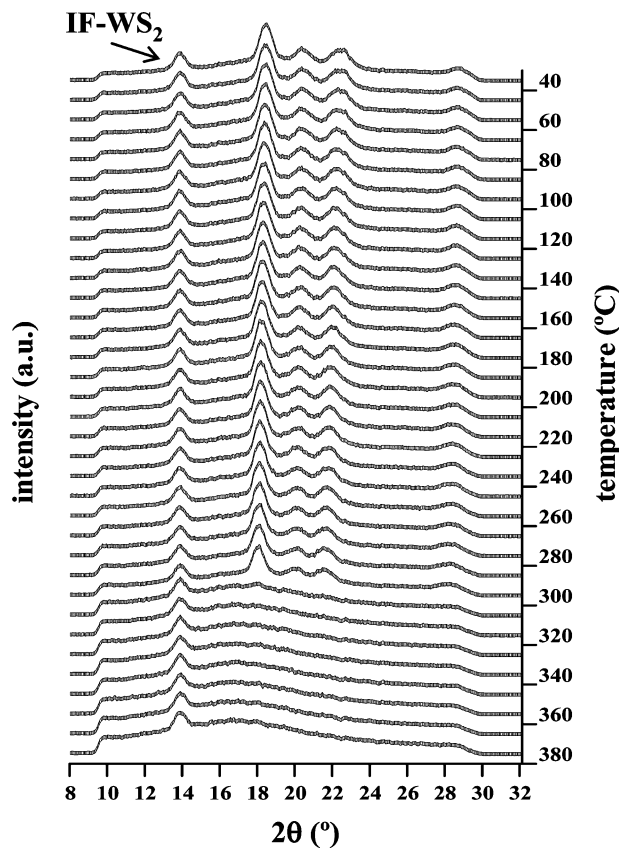


Figure 7. WAXS diffractograms of dynamic crystallization PEEK/IF-WS₂ (2 wt %) obtained during cooling at 10 °C/min.

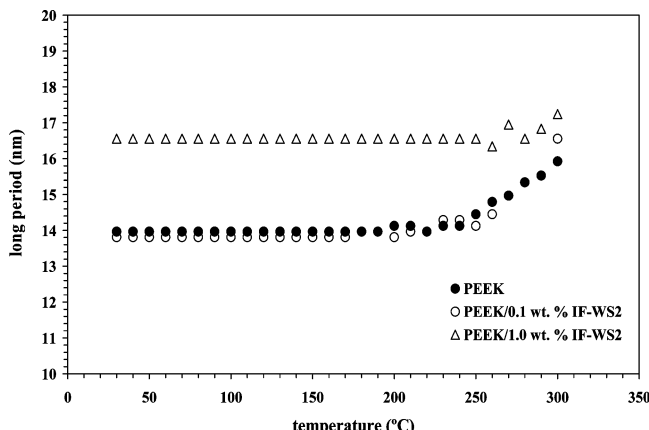


Figure 8. Long period (L) values of PEEK/IF-WS₂ nanocomposites obtained during cooling at 10 °C/min.

calculated from DSC curves (Figure 3). However, the crystalline structure of PEEK appears unchanged with the addition of IF-WS₂. Therefore, the changes in the crystallization parameters must be assigned to the nucleating efficiency of the IF-WS₂ nanoparticles. In addition to the above WAXS observation, the long period (L) values of PEEK in the nanocomposites have been obtained from the scattering maxima of real-time SAXS measurements. As an example, Figure 8 presents the temperature evolution of the long period (L) of PEEK and its nanocomposites obtained during cooling. If one takes into account the particle size of IF-WS₂ and the L values obtained, it seems evident to suggest that IF-WS₂ is absent from the interlamellar spaces of the PEEK crystals. Also, from the results of the L data, the possible role of the IF-WS₂ on the variation of thickness of the crystal lamellae of PEEK can be investigated. As noted

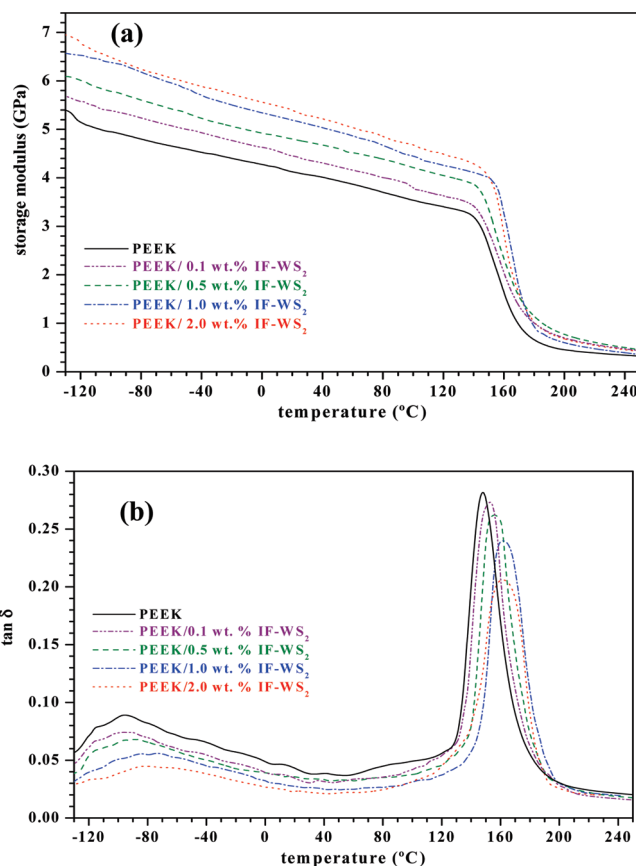


Figure 9. Dynamic mechanical analysis of PEEK/IF-WS₂ nanocomposites: (a) storage modulus versus temperature and (b) loss tangent versus temperature.

previously, L can be considered as the sum of the average thickness of the crystal lamellae and of the interlamellar amorphous regions. In addition, the parameter L and the crystallinity can also be used as a simple approximation to calculate the average thickness of the crystal lamellae of PEEK. Therefore, the increase of L value obtained at room temperature of the nanocomposite with 2 wt % of IF-WS₂ could be connected to the increase of the size of the crystallites of PEEK in the PEEK/IF-WS₂ nanocomposites, or in other words, the formation of more perfect crystals due to the reduction of the crystallization rate.

3.4. Mechanical Performance. 3.4.1. DMA Measurements.

Dynamic tests over a wide range of temperature and frequency are especially sensitive to all kinds of transitions and relaxation processes of the matrix and also to the morphology of the composites. An analysis of the storage modulus and $\tan \delta$ curves is very useful in ascertaining the performance of a sample under stress and temperature. Figure 9 shows the effect of the IF-WS₂ content on the storage and loss factor of PEEK. It is well-known that the dynamic storage modulus is very important in many structural applications. A clear understanding of the storage modulus–temperature curve obtained during a dynamic mechanical test provides valuable insight into the stiffness of a material. In the glassy region, the components are in a frozen state, i.e., highly immobile. In such a state, there exists a close and tight packing resulting in high modulus. As temperature increases, the components become more mobile and lose their close-packing arrangement. As a result, in the rubbery region there is a significant change in modulus. When the IF-WS₂ nanoparticles are incorporated, the stiffness of nanocomposites increases, resulting in higher storage modulus than the PEEK

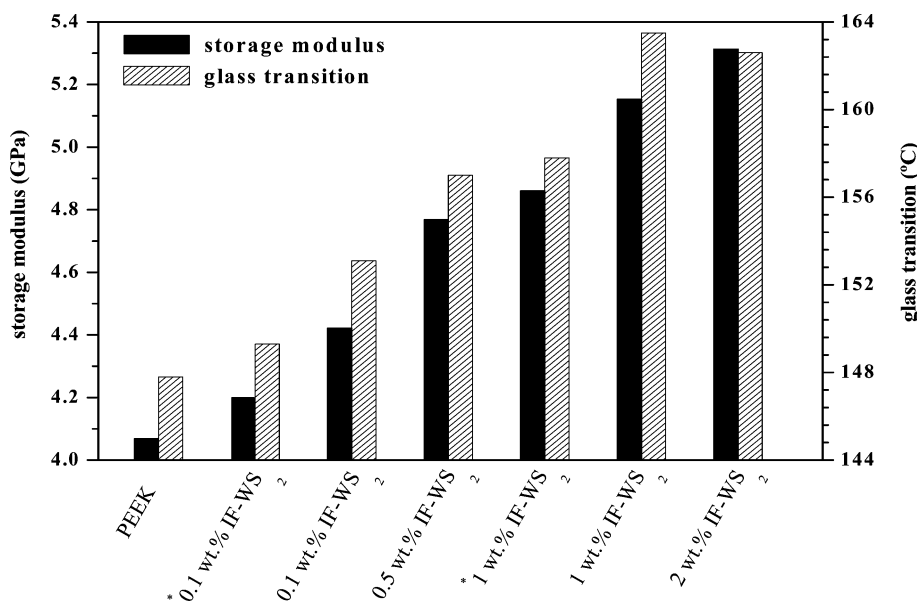


Figure 10. Room temperature values of storage modulus of PEEK/IF-WS₂ nanocomposites obtained at the frequency of 1 Hz versus IF-WS₂ concentration. (*) Nanocomposites obtained from direct mixing.

matrix. Thus, at room temperature, the addition of 0.1, 0.5, 1, and 2 wt % IF-WS₂ increases the storage modulus of the pure polymer (~ 4 GPa) by about 7, 16, 25, and 31%, respectively. The highest increment percentage obtained in these systems was observed for compatibilized PEEK/SWNT nanocomposites with 1 wt % of SWNT.^{28,30} However, the direct inclusion of 0.1 and 1 wt % IF-WS₂ has less reinforcing effect and only increased the modulus by ~ 2 and 18%, respectively (Figure 10).

The evolution of the loss factor ($\tan \delta$) as a function of temperature for PEEK and the nanocomposites is also shown in Figure 9b. Several relaxation peaks can be observed:³⁶ the maximum at lower temperatures (β relaxation) is related to local motions of the ketone groups, and the most intense peak (α relaxation) corresponds to the T_g of the materials (~ 148 °C for pure PEEK). The incorporation of nanoparticles results in a small reduction of the loss factor magnitude over the whole temperature range. With increasing IF-WS₂ content, all relaxation peaks broaden and shift to higher temperatures. The addition of 0.1, 0.5, 1, and 2 wt % IF-WS₂ increases T_g of the matrix by about 2, 6, 13, and 17 °C, respectively, whereas the direct integration of 0.1 and 1 wt % IF-WS₂ without the use of the predispersion step (Figure 9b) only rises it by 0.5 and 9 °C, respectively. In general, it has been established that the shift of T_g results from the contribution of the interaction between the dispersed phase and the matrix and the volume fraction of the resulting interface. Therefore, the remarkable temperature increment in the systems prepared by the combination of ball-milling and mechanochemical pretreatments in ethanol could be ascribed to the strong interaction induced by the improved filler dispersion and adhesion with the matrix attained by this procedure. On the other hand, the area and the magnitude of the α loss tangent peak is a reflection of polymer chain motion of amorphous phase. It can be observed from the figure that the height of the loss peak decreases with increasing nanoparticle concentration, pointing out this reduction in mobility caused by the addition of the IF-WS₂ nanoparticles. Moreover, the area under the loss peak is indicative of the energy dissipated in the viscoelastic relaxations. Samples containing small nanoparticle contents present similar area than the pure matrix. However, further increase in the concentration decreases this area, being the diminution about 18% for composites

including 2 wt % IF-WS₂ content. This decrease is less pronounced for nanocomposites prepared by direct mixing, indicating that the combination of melt blending with a premixing stage in an organic solvent improves the material stiffness without a detriment in its ability to dissipate energy.

3.4.2. Room Temperature Tensile Tests. Figure 11 shows the more representative tensile tests of PEEK/IF-WS₂ nanocomposites, and the tabulated data are summarized in Table 2. As shown in Figure 11a, all the studied materials present a linear elastic behavior at the beginning of tensile tests. The incorporation of nanofillers increases the Young's modulus of PEEK (4.1 GPa) by an average of 8, 19, 30, and 35% for loading fractions of 0.1, 0.5, 1, and 2 wt %, respectively (Figure 11b). In contrast, for composites prepared by direct mixing, the increments were only 5 and 23% for 0.1 and 1 wt % IF-WS₂. The improved behavior found for the former nanocomposites is attributed to a more efficient dispersion, hence larger interfacial area filler-matrix, as indicated by SEM observations. Our results reveal a nonlinear growth of the modulus with the filler content, the increase being more pronounced at low concentrations, in agreement with the behavior reported for PEEK composites reinforced by SWNT³⁷ and nanosized SiO₂ particulates.²⁷ The highest increment percentage obtained in these systems was observed for PEEK/SWNT (1 wt %) nanocomposites compatibilized with polysulfones (e.g., E (PEEK) ~ 4.1 GPa, E (PEEK/1 wt %) ~ 5.5 GPa)³⁷ as well as PEEK nanocomposites incorporating higher concentration of inorganic nanoparticles (e.g., E (PEEK) ~ 3.9 GPa and E (PEEK/10 wt % 30 nm Al₂O₃) ~ 5 GPa).³⁸

Focusing on the tensile strength (Figure 11c), experimental data reveal a continuous enhancement with increasing nanoparticle content. It increased by about 2, 6, 9, and 14% for composites including 0.1, 0.5, 1, and 2 wt % IF-WS₂ content in comparison to the pure PEEK (~ 129 MPa). However, in the studied range, the incorporation of nano-SiO₂ does not result in a pronounced modification in the tensile strength of PEEK.²⁷ On the other hand, the incorporation of IF-WS₂ does not result in a significant modification of the strain at yield for most of the samples tested. Moreover, the strain at break ($\sim 12\%$ for pure PEEK) slightly decreases up to loading fractions of 0.5 wt %, although it drops by about 36% for samples containing 2

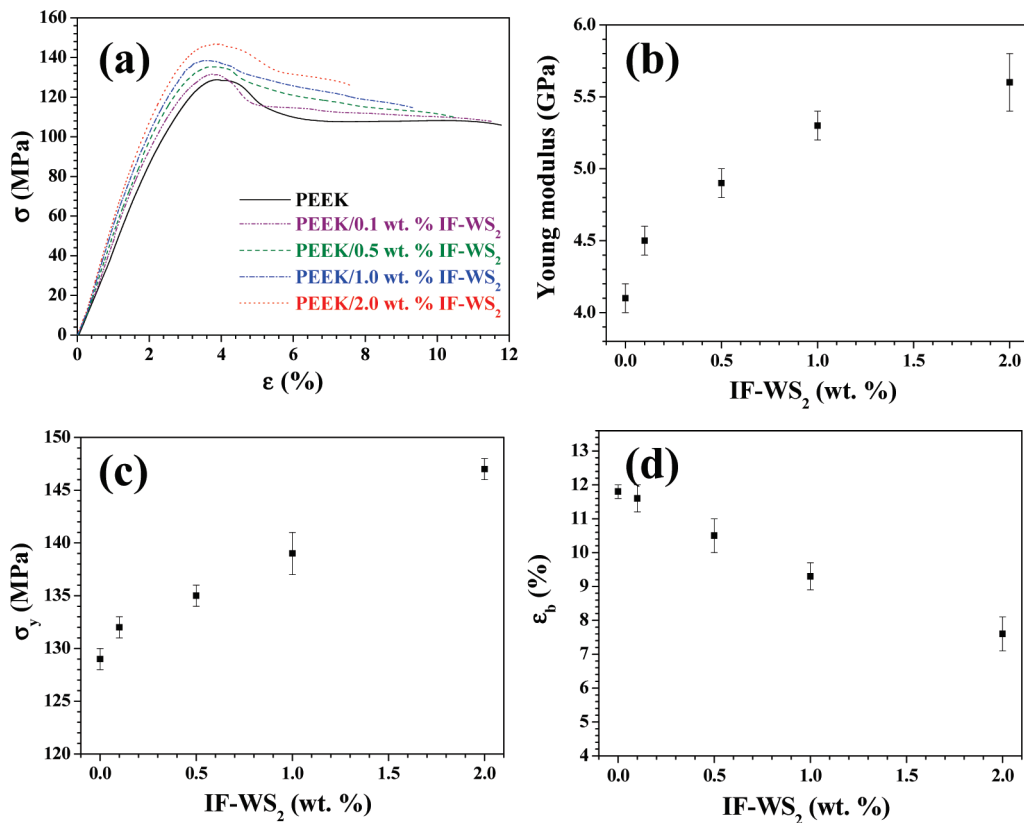


Figure 11. Tensile properties of PEEK/IF-WS₂ nanocomposites versus IF-WS₂ concentration: (a) representative stress–strain curves, (b) Young's modulus, (c) tensile strength, and (d) strain at break.

TABLE 2: Mechanical Parameters Derived from the Room Temperature Tensile and Charpy Impact Tests of PEEK/IF-WS₂ Nanocomposites^a

IF-WS ₂ content (%)	tensile tests					Charpy impact tests	
	E (GPa)	σ _y (MPa)	ε _y (%)	σ _b (MPa)	ε _b (%)	F (N)	E _{Charpy} (kJ/m ²)
0	4.1 ± 0.1	129 ± 1	4.0 ± 0.1	106 ± 1	11.8 ± 0.2	590 ± 20	5.9 ± 0.4
0.1	4.5 ± 0.1	132 ± 1	3.8 ± 0.1	109 ± 1	11.6 ± 0.4	720 ± 30	7.1 ± 0.9
0.5	4.9 ± 0.1	135 ± 1	3.7 ± 0.1	112 ± 1	10.5 ± 0.5	730 ± 50	6.3 ± 0.8
1	5.3 ± 0.1	139 ± 2	3.4 ± 0.1	115 ± 1	09.3 ± 0.4	630 ± 20	5.2 ± 0.5
2	5.6 ± 0.2	147 ± 1	3.6 ± 0.2	125 ± 1	07.6 ± 0.5	685 ± 30	4.4 ± 0.9
0.1 ^b	4.3 ± 0.1	131 ± 2	3.9 ± 0.1	109 ± 2	11.2 ± 0.3	480 ± 60	6.0 ± 1.0
1 ^b	5.1 ± 0.2	138 ± 1	3.5 ± 0.1	115 ± 2	08.7 ± 0.3	555 ± 40	4.0 ± 1.0

^a E, Young's modulus; σ_y, tensile strength at yield; ε_y, strain at yield; σ_b, tensile strength at break; ε_b, strain at break; F, impact force; and E_{Charpy}, impact strength. ^b Nanocomposites obtained from direct mixing.

wt % nanoparticle loading, indicating that higher filler contents restrict the ductile flow of the matrix (Figure 11d). Nevertheless, this restriction is considerably less drastic than the observed in PEEK composites reinforced with inorganic nanoparticles, where 1 wt % of SiO₂ and Al₂O₃ reduced the strain to failure by about 70 (i.e., from 9.5 to 3%) and 40% (i.e., from 12 to 7%), respectively.^{27,38} In the case of samples prepared by direct integration of the nanoparticles, the tensile failure elongation shows a strong drop (close to 35%) for 1 wt % particle loading. The drawn process is considerably more limited in these samples, probably presumably due to a small degree of particle agglomeration, which strongly obstructs the plastic deformation of the matrix.

The area under the tensile curve is a measure of the toughness of the system. In the nanocomposites containing well-dispersed IF-WS₂, this area was maintained up to loading fractions of 0.5 wt %, and then decreased slightly, the reduction being ~14 and 21% for samples loaded with 1 and 2 wt % IF-WS₂. However, for samples prepared by direct mixing containing 1 wt %

loading, the reduction is considerably stronger, close to 40%. Overall, the strength and toughness of the composites seem to be very sensitive to the state of dispersion of the filler and improve significantly in the samples prepared by dispersion in ethanol.

3.4.3. Charpy Impact Tests. Charpy notched impact strength measurements were carried out at room temperature to obtain more information about the toughness of the nanocomposites, and the results are also collected in Table 2. The incorporation of 0.1 and 0.5 wt % IF-WS₂ nanoparticles increases the impact strength of PEEK (~6 kJ/m²) by 20 and 7%, respectively, while higher loadings lead to a decrease of the toughness, the reduction being nearly 25% for samples including 2 wt % IF-WS₂ content. However, for nanocomposites prepared by direct mixing, the decrease was considerably stronger, consistent with the lower degree of plastic deformation of these composites as revealed by the tensile tests. This dependence of the impact strength on the IF-WS₂ content and the different behavior found for samples prepared by different procedures is in agreement with the

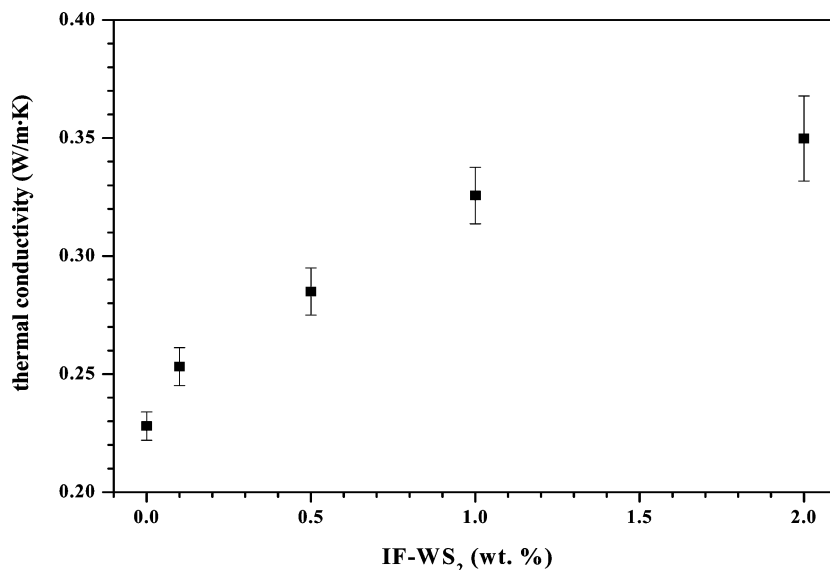


Figure 12. Thermal conductivity of PEEK/IF-WS₂ nanocomposites versus IF-WS₂ concentration.

analysis of the areas under the tensile curves. Furthermore, it is also consistent with the trends observed from the area under the loss factor peaks, since it is related to the energy dissipated in the viscoelastic relaxations, and any molecular process that promotes energy dissipation improves the impact resistance of the polymer.

As known, the shape, size, and state of dispersion of the filler and its interfacial adhesion with the matrix strongly condition the rate of energy absorption, hence the impact properties of polymer nanocomposites.^{6,37,39} The toughness of PEEK/IF-WS₂ nanocomposites improved noticeably by the mechanochemical pretreatments in ethanol, due to the more homogeneous filler dispersion which minimizes the stress concentration nuclei, as well as the enhanced interfacial adhesion that prevents the propagation of cracks. The incorporation of low content of other inorganic nanoparticles increased the tensile modulus of PEEK with the sacrifice of the matrix toughness and ductility. In contrast, the addition of IF-WS₂ provided a good balance between the stiffness and toughness. Moreover, the improvements in mechanical properties attained at 2 wt % IF-WS₂ content are similar to those achieved in composites including 1 wt % SWNT. This is highly interesting, since the inclusion of much cheaper nanoparticles in comparison to CNTs can lead to analogous enhancement in the strength and impact properties of these composites.

3.5. Thermal Conductivity. In order to analyze the influence of the nanoparticles on the thermal conductivity of PEEK, room temperature measurements were performed as a function of the IF-WS₂ content for all nanocomposites tested (Figure 12). The thermal conductivity is an important parameter that limits the cycle times in industrial injection processes. The thermal conductivity of PEEK ($0.23 \text{ W m}^{-1} \text{ K}^{-1}$) rises progressively with increasing nanoparticle loading, the increment being around 10, 27, 41, and 52% for samples including 0.1, 0.5, 1, and 2 wt % IF-WS₂. In contrast, for those prepared by direct mixing, the improvements for 0.1 and 1 wt % were only 5 and 30%, respectively. This indicates that the thermal conductivity is sensitive not only to the filler concentration but also to the state of dispersion of the filler. Similar trends were reported for PEEK/SWNT nanocomposites, although the improvements were larger in those samples, probably due to the larger conductivity of SWNTs in comparison to these nanoparticles.^{30,37} The increase of the thermal conductivity of PEEK in PEEK/IF-WS₂

nanocomposites can lead to a reduction in cycle times and therefore to greater processing efficiency during melt processing techniques like injection molding process.

4. Conclusions

In summary, we have demonstrated how IF-WS₂ nanofillers enable the preparation of advanced PEEK nanocomposite materials combining inorganic (which are known to be environmentally safe) and high-performance thermoplastic polymer using advantageously traditional melt processing technique (i.e., low-cost method). Bridging the surface energy gap between inorganic and organic constituents in composites has traditionally been achieved by chemical additives. Our present study shows how a predispersion processing step based on ball milling and mechanical treatments in organic solvent makes possible the integration of the IF WS₂ in the polymer matrix. This strategy provides a strong interaction induced by the improved filler dispersion and adhesion with the matrix attained by this procedure. An unprecedented shift in the initial degradation temperature of over 20 °C is obtained for PEEK at only 0.1 wt % of IF-WS₂, and with 2 wt % there is an improvement of nearly 60 °C under nitrogen atmosphere (55 °C in the case of air atmosphere). In the same manner, the incorporation of IF-WS₂ leads to an increase in the thermal conductivity of PEEK. On the other hand, dynamic mechanical analysis reveals a remarkable increase of the modulus and glass transition temperature of PEEK with the addition of IF-WS₂ due to the strong PEEK–particle interactions. However, the increase of concentration of IF-WS₂ leads to modifications of the crystallization behavior of the PEEK. The nucleation activity and effective energy barrier confirmed the unique dependence of the crystallization behavior of PEEK on composition. However, crystallinity and crystal structure of PEEK appear unchanged with addition of IF-WS₂. The overall mechanical performance demonstrates a good balance between the impact strength and stiffness of PEEK/IF-WS₂ nanocomposites as a lightweight alternative for use in critical applications, particularly for the aircraft industry.

Acknowledgment. M.N. expresses his sincere thanks to the Consejo Superior de Investigaciones Científicas (CSIC) for postdoctoral contract (I3PDR-6-02), financed by the European

Social Fund, and A.M.D.-P. thanks the Spanish Ministry of Science and Innovation for a postdoctoral Juan de la Cierva contract. This work was also supported by the European Union Sixth Framework Program (FOREMOST project under contract NMP3-CT-2005-515840), the European Commission for the X-ray synchrotron experiments performed at the Soft Condensed Matter A2 beamline at HASYLAB (DESY-Hamburg, 20090038 EC), and the coordinated project between the National Research Council of Canada (NRC) and the Spanish National Research Council (CSIC). The authors are also grateful to Dr. A. Johnston and Dr. B. Ashrafi for providing the opportunity to perform conductivity measurements at the NRC Institute of Aerospace Research (Canada).

References and Notes

- (1) Giannelis, E. P. *Adv. Mater.* **1996**, *8*, 29–35.
- (2) Jordan, J.; Jacob, K. I.; Tannenbaum, R.; Sharaf, M. A.; Jasiuk, I. *Mater. Sci. Eng., A* **2005**, *393*, 1–11.
- (3) Vaia, R. A.; Wagner, H. D. *Mater. Today* **2004**, *7*, 32–37.
- (4) Rozenberg, B. A.; Tenne, R. *Prog. Polym. Sci.* **2008**, *33*, 40–112.
- (5) Morgan, A. B. *Polym. Adv. Technol.* **2006**, *17*, 206–217.
- (6) Pavlidou, S.; Papaspyrides, C. D. *Prog. Polym. Sci.* **2008**, *33*, 1119–1198.
- (7) Caseri, W. *Chem. Eng. Commun.* **2009**, *196*, 549.
- (8) Tenne, R.; Margulis, L.; Genut, M.; Hodes, G. *Nature* **1992**, *360*, 444–445.
- (9) Hou, X.; Shan, C. X.; Choy, K. L. *Surf. Coat. Technol.* **2008**, *202*, 2287–2291.
- (10) Naffakh, M.; Martín, Z.; Fanegas, N.; Marco, C.; Gómez, M. A.; Jiménez, I. *J. Polym. Sci., Part B: Polym. Phys.* **2007**, *45*, 2309–2321.
- (11) Naffakh, M.; Martín, Z.; Marco, C.; Gómez, M. A.; Jiménez, I. *Thermochim. Acta* **2008**, *472*, 11–16.
- (12) Naffakh, M.; Marco, C.; Gómez, M. A.; Jiménez, I. *J. Phys. Chem. B* **2008**, *112*, 14819–14828.
- (13) Naffakh, M.; Marco, C.; Gómez, M. A. J.; Jiménez, I. *J. Phys. Chem. B* **2009**, *113*, 7107–7115.
- (14) Naffakh, M.; Marco, C.; Gómez, M. A.; Gómez-Herrero, J.; Jiménez, I. *J. Phys. Chem. B* **2009**, *113*, 10104–10111.
- (15) Tenne, R. *Nat. Nanotechnol.* **2006**, *1*, 103–111.
- (16) Katz, A.; Redlich, M.; Rapoport, L.; Wagner, H. D.; Tenne, R. *Tribol. Lett.* **2006**, *21*, 135–139.
- (17) Moore, G. E. “Acute inhalation toxicity study in rats - limit test. Product safety laboratories”. Study number 18503. Dayton, NJ, Jan 18 2006.
- (18) Denault, J.; Dumouchel, M. *Adv. Perform. Mater.* **1998**, *5*, 83–96.
- (19) Indu Shekar, R.; Kotresh, T. M.; Damodara Rao, P. M.; Kumar, K. *J. Appl. Polym. Sci.* **2009**, *112*, 2497–2510.
- (20) Weidig, R. *Kunstst-Plast. Eur.* **2001**, *91*, 64–65.
- (21) Drioli, E.; Regina, A.; Casciola, M.; Oliveti, A.; Trotta, F.; Massari, T. *J. Membr. Sci.* **2004**, *228*, 139–148.
- (22) Kurtz, S. M.; Devine, John N. *BioMater.* **2007**, *28*, 4845–4869.
- (23) Naffakh, M.; Ellis, G.; Gómez, M. A.; Marco, C. *Polym. Degrad. Stab.* **1999**, *66*, 405–413.
- (24) Naffakh, M.; Gómez, M. A.; Marco, C.; Ellis, G. *Polym. Eng. Sci.* **2006**, *46*, 129–138.
- (25) Maser, W. K.; Benito, A. M.; Castel, P.; Sainz, R.; Martínez, M. T.; Naffakh, M.; Marco, C.; Ellis, G.; Gómez, M. A. *Carbon nanotube composite materials: opportunities and processing issues*. NATO Science for Peace and Security Series, B: Physics and Biophysics. Nanostructured Materials for Advanced Technological Applications; Reithmaier, J. P., Petkov, P., Kulisch, W., Popov, C., Eds.; 2009, pp 181–198. DOI: 10.1007/978-1-4020-9916-8_18
- (26) Naffakh, M.; Marco, C.; Gómez, M. A.; Ellis, G.; Maser, W. K.; Benito, A. M.; Martínez, M. T. *J. Nanosci. Nanotechnol.* **2009**, *9*, 6120–6126.
- (27) Zhang, G.; Schlarb, A. K.; Tria, S.; Elkedi, O. *Compos. Sci. Technol.* **2008**, *68*, 3073–3080.
- (28) Díez-Pascual, A. M.; Naffakh, M.; González-Domínguez, J. M.; Martínez-Rubi, Y.; Ansón, A.; Martínez, M. T.; Simard, B.; Gómez, M. A. *Carbon* **2010**, *48*, 3485–3499.
- (29) Díez-Pascual, A. M.; Naffakh, M.; Gómez, M. A.; Marco, C.; Ellis, G.; Martínez, M. T.; Ansón, A.; González-Domínguez, J. M.; Martínez-Rubi, Y.; Simard, B. *Carbon* **2009**, *47*, 3079–3090.
- (30) Díez-Pascual, A. M.; Naffakh, M.; Gómez, M. A.; Marco, C.; Ellis, G.; González-Domínguez, J. M.; Ansón, A.; Martínez, M. T.; Martínez-Rubi, Y.; Simard, B.; Asharfi, B. *Nanotechnology* **2009**, *20*, 315707.
- (31) Dobrev, A.; Gutzow, I. *J. Non-Cryst. Solids* **1993**, *162*, 1–12.
- (32) Dobrev, A.; Gutzow, I. *J. Non-Cryst. Solids* **1993**, *162*, 13–25.
- (33) Kissinger, H. E. *J. Res. Natl. Bur. Stand.* **1956**, *57*, 217–221.
- (34) Dawson, P. C.; Blundell, D. J. *Polymer* **1980**, *21*, 577–578.
- (35) Rueda, D. R.; Ania, F.; Richardson, A.; Ward, I. M.; Baltá-Calleja, F. *J. Polym. Commun.* **1983**, *24*, 258–260.
- (36) Goodwin, A. A.; Hay, J. N. *J. Polym. Sci., Part B: Polym. Phys.* **1998**, *36*, 851–859.
- (37) Díez-Pascual, A. M.; Naffakh, M.; González-Domínguez, J. M.; Martínez-Rubi, Y.; Ansón, A.; Martínez, M. T.; Simard, B.; Gómez, M. A. *Carbon* **2010**, *48*, 3500–3511.
- (38) Kuo, M. C.; Tsai, C. M.; Huang, J. C.; Chen, M. *Mater. Chem. Phys.* **2005**, *90*, 185–195.
- (39) Chena, B.; Evans, J. R. G. *Soft Matter* **2009**, *5*, 3572–3584.

JP105340G